International Journal of Information Technology & Computer Engineering

ISSN 2347–3657

Volume 14, Issue 1, 2026

Assessing Evapotranspiration In Wheat Crop Using METRIC Model In Karnal District Of Haryana

Ankush Khatkar[1], Annu[2], Dharmendra singh[2], Harinarayanan.M. N[2]

[1,2]Haryana Space Applications Centre

[1]Email: ankushkhatkar268@gmail.com

Abstract

Sustainable agriculture requires efficient water management, particularly for water-intensive crops such as wheat. This study applies the METRIC (Mapping Evapotranspiration at High Resolution with Internalized Calibration) model to estimate actual evapotranspiration (ETa) in the wheat-growing regions of Karnal district, Haryana. A wheat crop mask was extracted and combined with satellite-derived indices (NDVI, SAVI, LST, LAI, and albedo), DEM, and meteorological data to compute surface energy fluxes and ETa. Field-based pan evaporation with crop coefficients (Kc) data was also used to estimate ETa for comparison. Results showed that pan-based ETa increased gradually with accordance to the growth stages of wheat and declined further. Validation against FAO Penman-Monteith Kc-based ETc showed moderate to strong agreement (R^2 = 0.68), with RMSE of 0.824 mm day^{-1} and MAE of 0.609 mm day^{-1}. The METRIC model effectively captured temporal and spatial variation in wheat ETa across growth stages. Findings demonstrate METRIC's reliability for water budgeting and irrigation scheduling, supporting precision agriculture and improved water productivity in semi-arid regions.

Keywords: *METRIC, evapotranspiration, wheat, remote sensing, Karnal, irrigation scheduling, water productivity*

1. Introduction

Agriculture is a cornerstone of the Indian economy, contributing significantly to employment, food security and GDP. Among the major agricultural states, Haryana holds a pivotal position due to its high agricultural productivity and extensive wheat cultivation (Bhupal, D. S. 2012). Wheat is a staple food crop in India and occupies a central position in the country's food security. India is the second-largest producer of wheat globally, and the northern plains, particularly the state of Haryana, are significant contributors to national wheat production (Singh et al., 2020). Wheat, a water-intensive crop, requires efficient water management practices to ensure optimal yield and sustainability. The Karnal district, situated in the Indo-Gangetic plains, is a major wheat-growing region owing to its fertile soil, favorable agro-climatic conditions, and access to irrigation. However, increasing pressure on water resources due to intensive cropping demands accurate water use estimation and management.

In this context, evapotranspiration (ET) emerges as a critical factor, representing the combined processes of water loss through soil evaporation and plant transpiration. Accurate estimation and management of ET are essential for optimizing irrigation, improving water use efficiency and mitigating the adverse effects of water scarcity (Allen et al., 1998). Evapotranspiration (ET), which combines the processes of soil evaporation and plant transpiration, is a critical component of the hydrological cycle. Accurate estimation of ET is vital for efficient irrigation scheduling, crop water budgeting, and sustainable water resource management, especially in regions facing water scarcity (Allen et al., 2007). In arid and semi-arid areas, where agriculture heavily relies on irrigation, ET plays a pivotal role in determining crop water requirements and optimizing water use efficiency (Bastiaanssen et al., 1998).

Traditional methods of estimating ET using lysimeters or empirical equations like Penman-Monteith are spatially limited and data-intensive. Remote sensing, integrated with Geographic Information System (GIS), provides an efficient and scalable alternative to estimate ET over large agricultural landscapes (Glenn et al., 2007). Satellite imagery enables the derivation of key surface parameters such as surface temperature, albedo, vegetation indices, and net radiation, which are used in energy balance models to calculate ET at high spatial and temporal resolutions. They help monitor agricultural water use, climate variability and environmental sustainability over large areas with precision and efficiency (Senkondo et al., 2019). Remote sensing-based approaches, such as the METRIC model (Mapping Evapotranspiration at High Resolution with Internalized Calibration) model, offer a robust alternative. These models integrate satellite imagery with meteorological data to provide spatially distributed ET estimates, enabling precision agriculture (Allen et al., 2007).

The METRIC (Mapping Evapotranspiration at high Resolution with Internalized Calibration) model is a satellite-based surface energy balance algorithm that estimates ET using remote sensing data, incorporating ground-based weather inputs for calibration (Allen et al., 2007). Unlike other models, METRIC internally calibrates using "hot" and "cold" pixels representing extremes of ET in the image scene, thereby improving the accuracy and reducing dependency on extensive ground data (Tasumi et al., 2005). The model has been successfully applied in various regions to assess

International Journal of Information Technology & Computer Engineering
ISSN 2347–3657
Volume 14, Issue 1, 2026

field-scale water consumption and irrigation performance. The METRIC model has been used in studies in Saudi Arabia to assess potential evapotranspiration in cities, aiming to improve irrigation planning, water use monitoring and promote sustainable agricultural practices in arid and semi-arid regions (Islam et al., 2015).

Therefore, the present study focuses to estimate actual evapotranspiration in wheat crop using the METRIC model and demonstrate the utility of remote sensing-based ET estimation for efficient irrigation and water resource planning in Haryana.

2. Study Area

Karnal district is situated in the northern part of Haryana state in India and forms part of the agriculturally rich Indo-Gangetic Plains. The region is known for its intensive agriculture, supported by fertile alluvial soils and a well-developed irrigation infrastructure. The district lies between 29°09′ N to 29°59′ N latitude and 76°31′ E to 77°12′ E longitude, covering an area of approximately 2,520 square kilometers.

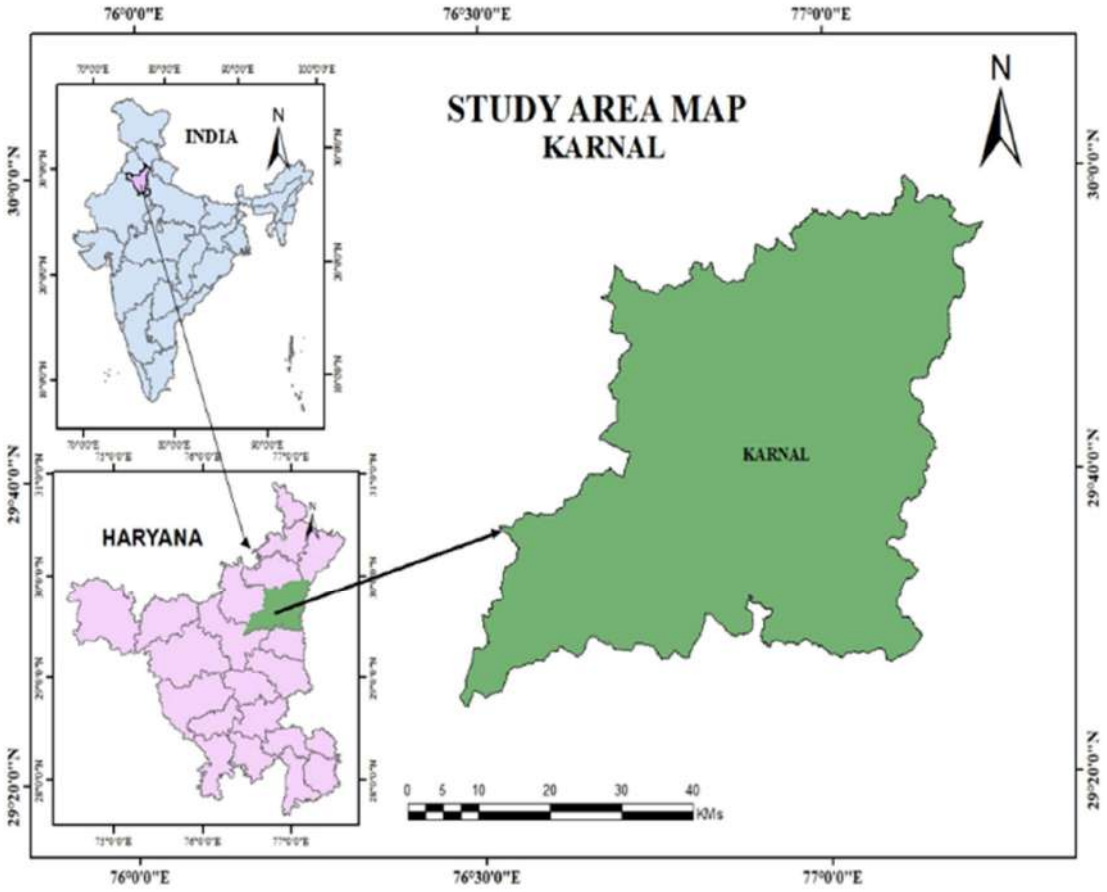

Figure 1 Study Area

It shares boundaries with Kurukshetra district in the north, Panipat in the south, and Uttar Pradesh state to the east, across the Yamuna River. The elevation ranges from 235 to 252 meters above sea level. Karnal falls under the Trans-Gangetic Plains Region and is classified as a sub-tropical, semi-arid zone. The region experiences hot summers and cool winters, with an average annual temperature ranging between 7°C in January to 45°C in June. The average annual rainfall is around 700–800 mm, the majority of which occurs during the southwest monsoon season from July to September. Groundwater and canal systems are the main sources of irrigation. These climatic and soil conditions are conducive for the cultivation of wheat and other Rabi crops. The dominant cropping pattern in Karnal is the rice–wheat rotation, practiced on a large scale due to assured irrigation and high productivity. Wheat is sown typically in November and harvested in April. The region is characterized by high-input farming practices and intensive irrigation, which makes it an ideal location for evaluating actual water consumption by crops. The study area map was given as Figure 1 for the reference.

3. Methodology

The experiment was conducted at Haryana Space Applications Centre, Gurugram lab. The study utilizes various remote sensing products from MODIS, Sentinal and ERA 5 to estimate the ET for the given region. The inputs from various satellite

International Journal of Information Technology & Computer Engineering
ISSN 2347–3657
Volume 14, Issue 1, 2026

data products were integrated with the help of Google Earth Engine (GEE).

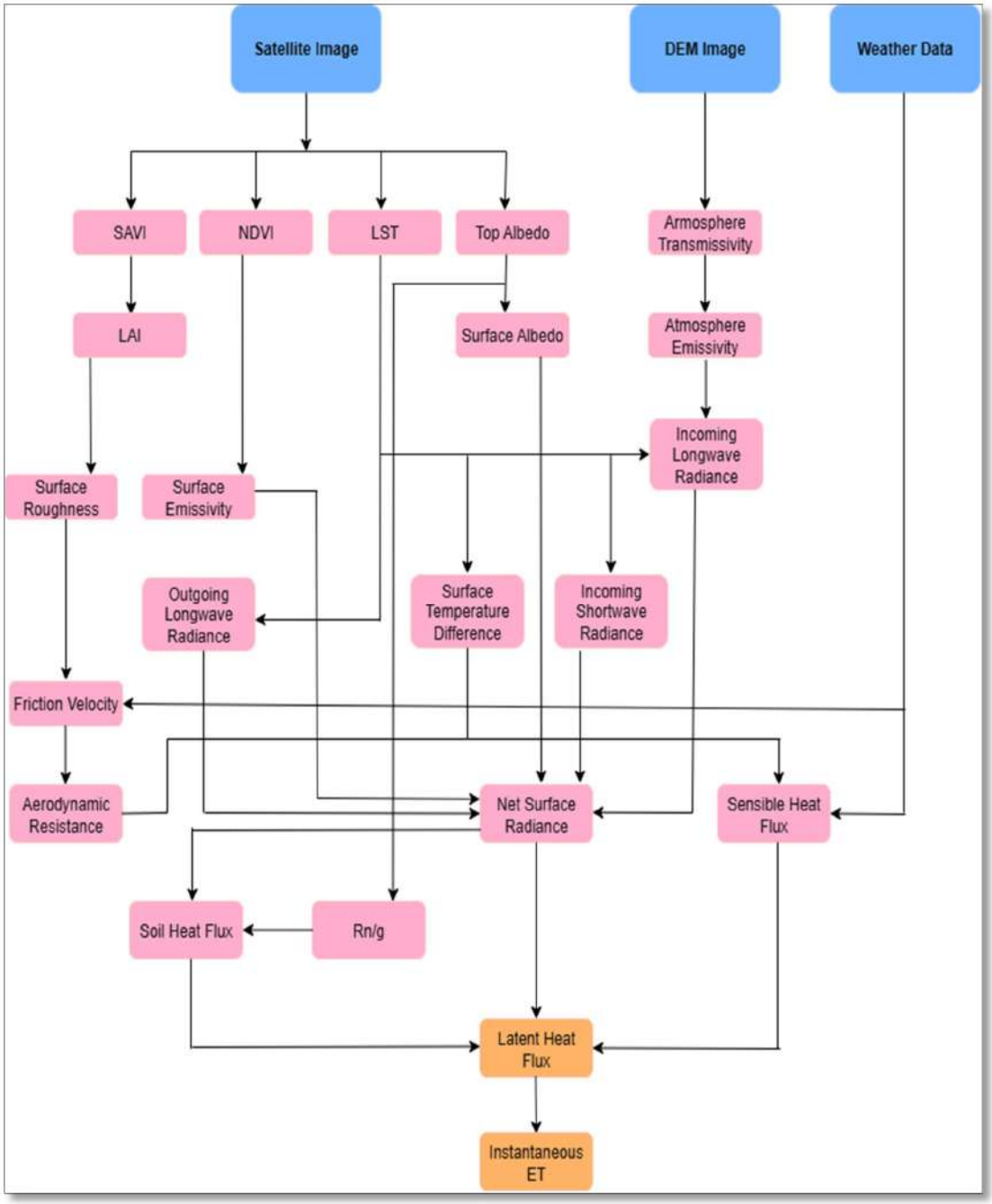

Figure 2 Methodology of ET Estimation through METRIC Model

The meteorological parameters were collected from the meteorological observatory located at the Central Soil Salinity Research Institute (CSSRI) as well as from ERA-5 satellite data. A wheat mask of the study area was obtained for the precise estimation of METRIC ET. The reference evapotranspiration and actual ET were calculated based on crop coefficient approach using the station observed meteorological data to validate the METRIC estimated ET. The detailed methodology for computing METRIC ET was described as a flowchart in Figure 2 and the methodology for deriving reference ET from station data was illustrated in subsequent flowchart, mentioned as Figure 3.

International Journal of Information Technology & Computer Engineering
ISSN 2347–3657
Volume 14, Issue 1, 2026

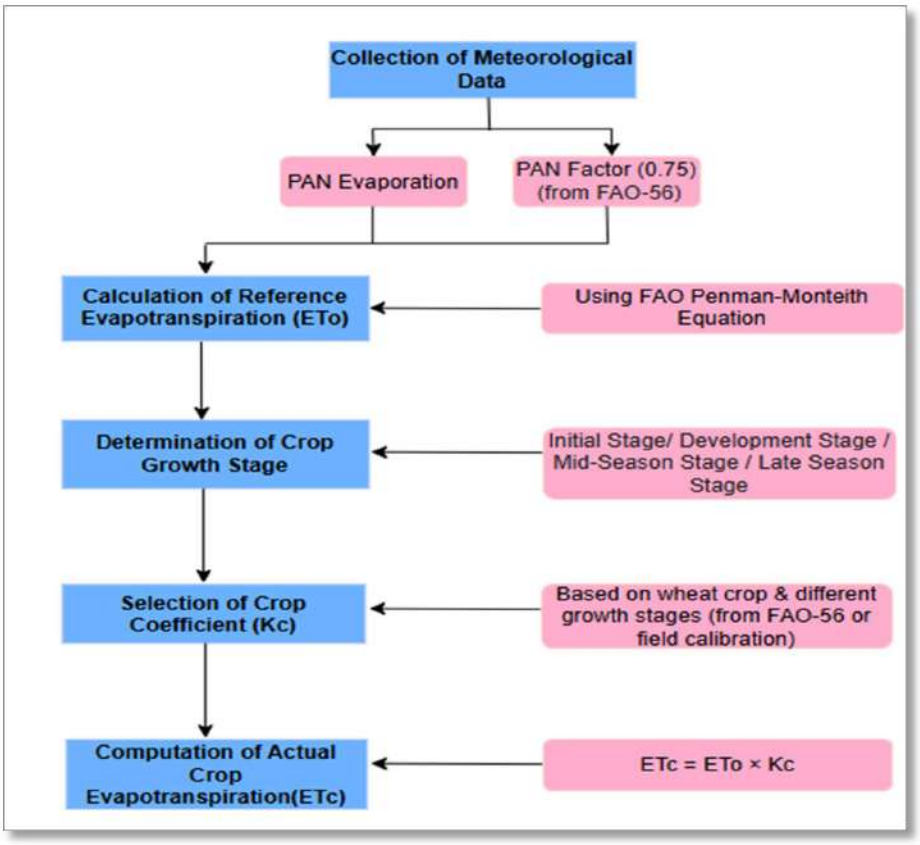

Figure 3 Methodology of ET Estimation through Crop Coefficient Approach

3.1. Data and Software Used

Various satellite data products were utilized in this study to calculate the input parameters needed to run the METRIC model. These data were integrated using Google Earth Engine (GEE) and the further analysis was done by employing GIS software and tools. The detailed list of data and software used were given in Table 1 and Table 2 respectively.

Table 1 Data and Used for the Study

Satellite/Ground Software Name	Resolution Work	Source
Landsat-8 OLI	30-metre	https://earthexplorer.usgs.gov/
ArcGIS	Raster calculation, mosaic	
Sentinel-2	4 bands at 10 m, 6 bands at 20 m, 3 bands at 60 m	https://scihub.copernicus.eu/
Erdas Imagine	Classification, accuracy assessment, mosaic, subset, layer stack, reprojection,	
Google Earth Engine	Sentinel -2 image download, NDVI stack image download	
DEM Data	30 metre	https://earthexplorer.usgs.gov/
MS Excel 2021	Statistical Analysis	
Meteorological Data		ERA 5 – https ://cds.climate.copernicus.eu/
Wheat Mask of AOI		Haryana Space Applications Centre (HARSAC)

Table-2: Software and Tools Used for the Study

3.2. Parameters Description

3.2.1. Soil Adjusted Vegetation Index

Soil adjusted vegetation index is a vegetation index used to quantify vegetation cover in those area where reflectance values effected by soil background (Allen et al., 2002).

SAVI : *((NIR - Red) / (NIR + Red + L)) * (1 + L), where L = 0.5*

Where RED or NIR are the reflectance, L is the parameter which is constant values. There are three values of L (0.2, 0.5. 0.9) which areas of soil calculation.

3.2.2. Normalized Difference Vegetation Index

Normalized Difference Vegetation Index is most widely used health condition and quantity of vegetation. NDVI was introduced by Rousil (1973), NDVI algorithm based on vegetation phenology as the green vegetation reflects less in visible light and more in NIR where sparse vegetation reflects a great portion of visible and less portion of NIR (Allen et al., 2002).

NDVI : *(NIR - Red) / (NIR + Red)*

3.2.3. Land Surface Temperature

Land surface Temperature represent the temperature of the Earth's surface. LST is one of key parameter that effect surface energy balance, climates, heat fluxes and energy exchanges LST is obtained using thermal infrared remote sensing, which measures the thermal radiation emitted by the Earth's Surface (Allen et al., 2002).

LST : *(TIR * 0.03418) + 149.0 - 273.15*

3.2.4. Top Albedo

The term "Top Albedo" refers to the albedo of earth topmost layers which refers to the albedo of earth surface. Top of Atmosphere Albedo is defined as the fraction of incoming solar radiation that reflected by the Earth atmosphere system back to space at the top boundary of the atmosphere (Roy et al.,2014).

Top Albedo: *(0.356*B2 + 0.130*B4 + 0.373*B5 + 0.085*B6 + 0.072*B7) - 0.018*

3.2.5. Leaf Area Index

Leaf Area Index is a important biophysical variable. LAI directly affect the interception of solar radiation, canopy resistance, and surface balance energy which in turn effect both transpiration and evaporation. LAI represents the total one sided leaf area provides per unit ground area and provides information about the amount of leaf surface available for photosynthesis (Allen et al., 2002).

LAI: *ln (0.69 - SAVI) / 0.59*

3.2.6. Surface Albedo

The percentage of incoming solar radiation (shortwave) that a surface reflects is known as surface albedo, and it is a crucial element in the Earth's surface energy balance. A ratio between 0 and 1 is used to express this dimensionless quantity A surface with an albedo of 0 is said to be black since it absorbs all incoming solar radiation (no reflection). Like fresh snow or a mirror, a surface with an albedo of 1 reflects all incoming solar radiation(no absorption). Surface type, moisture content, incoming radiation angle, vegetation cover, and atmospheric conditions all affect albedo; it is not a constant feature (Tasumi et al. 2007).

Surface Albedo : *0.254*B2 + 0.149*B4 + 0.147*B5 + 0.311*B6 + 0.103*B7 + 0.036*

3.2.7. Surface Roughness for Momentum Transport

The texture and irregularity of the Earth's surface are referred to as surface roughness, and they have an impact on the movement of heat, moisture, and momentum between the atmosphere and the land. The aerodynamic roughness length (z_0), a theoretical height at which wind speed drops to zero in neutral conditions, is used to measure it. Surface type affects roughness length; it is shorter on smooth surfaces, such as water, and longer on vegetated or urban areas. It has a significant impact on surface energy balance and evapotranspiration calculations in micrometeorology and models such as METRIC (Allen et al., 2002).

Surface Roughness: *(5.357 * NDVI) - 2.809*

3.2.8. Outgoing Longwave Radiation

The energy sent into space by the Earth's atmosphere and surface, mostly in the thermal infrared spectrum, is known as outgoing longwave radiation. It displays the emissivity and temperature of the Earth's surface. This radiation is essential to Earth's cooling and radiation budget. In remote sensing for land surface temperature research, its estimation is crucial (Allen et al., 2002).

Outgoing Longwave Radiation : $\varepsilon \times \sigma \times LST^4$,

Where, $\varepsilon = 0.99$ if NDVI > 0.5, $\varepsilon = 0.96$ if NDVI < 0.2, $\varepsilon = 0.004 \times PV + 0.986$ if $0.2 \leq NDVI \leq 0.5$, and $PV = ((NDVI - 0.2)/(0.5 - 0.2))^2$, $\sigma = 5.67 \times 10^{-8}$ W·m−2·K−4

3.2.9. Friction Velocity

A measure of turbulent momentum transfer in the atmospheric boundary layer, friction velocity is a function of the shear stress that the wind applies to the surface. It is based on the surface's roughness properties and wind speed profile. Friction velocity is commonly employed in evapotranspiration and energy balance models and is essential in micrometeorology for estimating heat, moisture, and momentum fluxes (Allen et al., 2002).

Friction Velocity : $u^* = (\kappa \times u) / \ln(z/z0)$,

where $\kappa = 0.4$ (von Kármán constant), $z = 10m$ (measurement height), $z0 = 0.1m$ (roughness length), and $u = \sqrt{(u^2 + v^2)}$ (wind speed), where u^2 is zonal wind and v^2 is meridional wind

3.2.10. Near Surface Temperature Difference

The near-surface temperature difference refers to the temperature contrast or variation observed within a relatively close proximity to the Earth's surface. It is typically measured or estimated between different levels near the ground, such as the air temperature at the surface and at a certain height above the surface. The unit of Near Surface Difference Temperature is k. Low differences indicate moist/cool surfaces, while high gradients (~3–5°C) enhance flux calculations (Liu et al., 2021).

Near Surface Temperature Difference : $(a + bT_s)$

Where, Ts is the temperature (k). a and b have to find from albedo and surface roughness trend line.

3.2.11. Net Surface Radiation

The total of all incoming and outgoing radiative fluxes at the Earth's surface is known as net surface radiation. It is a major force behind surface energy processes including heating, evapotranspiration, and photosynthesis and represents the energy that is available at the interface between the land and the atmosphere. Net radiation is "the difference between

International Journal of Information Technology & Computer Engineering
ISSN 2347–3657
Volume 14, Issue 1, 2026

all incoming and outgoing radiation fluxes at a surface and indicates the energy available for non-radiative activities," according to Monteith and Unsworth (1990).

Usually expressed in watts per square meter (W/m2), net radiation is affected by a number of variables, including land use, cloud cover, meteorological conditions, and surface albedo. Energy gain is shown by positive net radiation, whereas net energy loss from the surface is suggested by negative readings (Allen et al., 2002).

Net Surface Radiation : *Rn = Rs_in - Rs_out - Rnl_out,*

where Rs_in = incoming shortwave radiation, Rs_out = α × Rs_in (α = 0.254×B2 + 0.149×B3 + 0.147×B4 + 0.311×B5 + 0.103×B6 + 0.036×B7), and Rnl_out = ε × σ × T⁴ (ε = 0.97, σ = 5.67e-8)

3.2.12. Aerodynamic Resistance

Aerodynamic resistance refers to the resistance of turbulent flow in the atmosphere to the transfer of mass, heat, or momentum (like water vapor) between the Earth's surface and the atmosphere.

It is essential to evapotranspiration calculations and surface energy balance models. Air and energy can flow between the surface and the atmosphere more readily when the aerodynamic resistance is reduced.

Aerodynamic Resistance: $r_a = ln((z - d) / z_0) / (k \times u)$,

where z = reference height (10 m), d = displacement height (d = 1.675 × z₀), z₀ = surface roughness length (from LAI), k = von Kármán constant (0.41), and u = friction velocity (u = (k × u) / ln (z / z₀))

3.2.13. Soil Heat Flux

Soil heat flux refers to the flow of heat through the soil. Soil heat flux is an important component of the energy balance of the Earth's surface and plays a crucial role in processes such as soil temperature regulation, plant growth, and the exchange of energy between the land surface and the atmosphere. The unit of soil heat flux is w/m² (Yang et al., 2019).

Soil Heat Flux : G = C × Rn,

where C = 0.31 (empirical coefficient) and Rn = (1 - α) × Rs (Rs = incoming solar radiation, α = surface albedo)

3.2.14. Sensible Heat Flux

It refers to the transfer of heat between the Earth's surface and the atmosphere through conduction and convection processes. When there is a temperature gradient between the Earth's surface and the overlying air, heat is transferred from the warmer surface to the cooler air or vice versa *(Mondal et al., 2019)*. This transfer of heat is referred to as sensible heat flux. It is called "sensible" because it can be sensed or felt as a change in temperature. The unit of sensible heat flux is W/m²(Liu Shaomin et al., 2007).

Sensible Heat Flux : *H = (ρ × cp × dT) / rah*

where ρ = 1.225 kg/m³ (air density), cp = 1004 J/kg·K (specific heat), dT = 0.2 × (LST - meanLST) (temperature difference), and rah = min(208/windSpeed, 50) (aerodynamic resistance)

3.2.15. Latent Heat Flux

In the context of evapotranspiration, the latent heat flux refers to the energy transfer associated with the conversion of liquid water into water vapor during the processes of evaporation and transpiration. Evapotranspiration is influenced by various factors, including solar radiation, air temperature, humidity, wind speed, vegetation type, and soil moisture content. The unit of Sensible Heat Flux is W/m² (Castellvi et al., 2022).

Latent Heat Flux: *Rn - G – H*

3.2.16. Instantaneous ET

Instantaneous ET refers to the measurement or estimation of evapotranspiration at a specific moment or point in time. Understanding instantaneous ET is important in various fields, particularly in agriculture, hydrology, and environmental studies. By knowing the instantaneous ET rate, farmers can make informed decisions regarding irrigation scheduling, allowing them to provide the right amount of water to crops precisely when needed (Allen et al., 2002).

Instantaneous ET : *(LE × 3600) / λ*

3.2.17. Actual ET

The total amount of water that is moved from the land surface to the atmosphere by the combined processes of transpiration from plant tissues and evaporation from soil and plant surfaces is known as actual evapotranspiration, or Evapotranspiration. In contrast to potential evapotranspiration, which is based on the assumption of an infinite water supply, Evapotranspiration represents the actual water loss that takes place under current climatic, soil moisture, and vegetation conditions.

$$ETa = \sum_{i=m}^{n}[(ETrFi)(ETr24i)]$$

Where, ETa = Actual ET for 24 hours

ETrF is the reference ET fraction and ETr24is a summation of ETr values of a day (mm day−1).

3.3. ET Based On Crop Coefficient Approach

In the crop coefficient approach the crop evapotranspiration, ET_c, is calculated by multiplying the reference crop evapotranspiration, ET_o, by a crop coefficient, K_c:

$ET_c = K_c\ ET_o$ (FAO 56)

Where, ET_c crop evapotranspiration [mm d^{-1}], K_c crop coefficient [dimensionless], ET_o reference crop evapotranspiration [mm d^{-1}].

The crop coefficients of wheat, for different growth stages were referenced from the FAO and given in Table 3.

Table 3 Crop Coefficients of wheat

Sl No.	Stage of Crop	Kc Value
1	Initial Stage	0.7

International Journal of Information Technology & Computer Engineering
ISSN 2347–3657
Volume 14, Issue 1, 2026

2	Mid-season	1.15
3	Late Season/Harvest	0.25

3.4. Comparison of ETa Estimation Methods

3.4.1. RMSE (Root Mean Square Error)

By taking the square root of the mean of squared differences between observed (yi) and estimated (Þi) values, the Root Mean Square Error (RMSE) calculates the average magnitude of the prediction error. It works well for identifying notable variations in Evapotranspiration estimation because of its high sensitivity to large errors. Higher model accuracy and improved agreement with reference or groundtruth data are indicated by lower RMSE values.

$$RMSE = \sqrt{MSE} = \sqrt{((1/N) * \Sigma (yi - \hat{y}i)^2)}$$

3.4.2. Mean Absolute Error (MAE)

An intuitive understanding of model performance is provided by the Mean Absolute Error (MAE), which calculates the average absolute variations between observed and predicted values. In contrast to RMSE, MAE does not assign greater weight to larger deviations; instead, it treats all errors equally. When comparing various estimation models in terms of consistent bias in Evapotranspiration predictions, it is particularly helpful.

$$MAE = (1 / N) * \Sigma |yi - \hat{y}i|$$

3.4.3. Coefficient of determination

The percentage of variance in observed Evapotranspiration that can be accounted for by the model is measured by the coefficient of determination (R^2). Higher levels of correlation and a better model fit are indicated by an R^2 value nearer 1. In Evapotranspiration studies, it is frequently used to assess how well empirical or remote sensing-based models reproduce real-world field observations.

$$R^2 = 1 - [\Sigma (yi - \hat{y}i)^2] / [\Sigma (yi - \bar{y})^2]$$

4. Results

4.1. Estimation of instantaneous ET

The estimated instantaneous ET from November to January was displayed in Fig. 4a and following March to April was displayed on Fig 4b. On 10 November, Instant ET values range between 3.62–5.38 mm/hr, indicating active evapotranspiration during the early growth stage. The higher values reflect sufficient soil moisture and initial crop establishment. On 26 November, Instant ET drops to 2.18–3.63 mm/hr, suggesting a temporary decline in crop water use. This reduction may be due to cool weather conditions or slower vegetative growth. On 13 January, Instant ET increases significantly ranging 3.49–5.76 mm/hr, indicating peak vegetative growth. This reflects high transpiration due to a well-developed canopy and optimal weather conditions. On 29 January, Instant ET ranges from 2.90–4.56 mm/hr, marking a shift from vegetative to reproductive stages. Slightly reduced values suggest moderate water use efficiency during this transitional phase. On 2nd March, Instant ET ranged between 0.40–0.47 mm/hr, possibly due to conversion from energy units. The values correspond to high actual ET during the grain-filling stage, when water demand peaks. On 18 March, Instant ET decreases to 0.18–0.40 mm/hr, reflecting reduced crop water use during the maturity phase. This stage is characterized by declining LAI and lower transpiration. On 3 April, Instant ET values further reduce to 0.09–0.26 mm/hr, indicating less evapotranspiration as the crop reaches senescence. This marks the end of the growing season and near-harvest conditions.

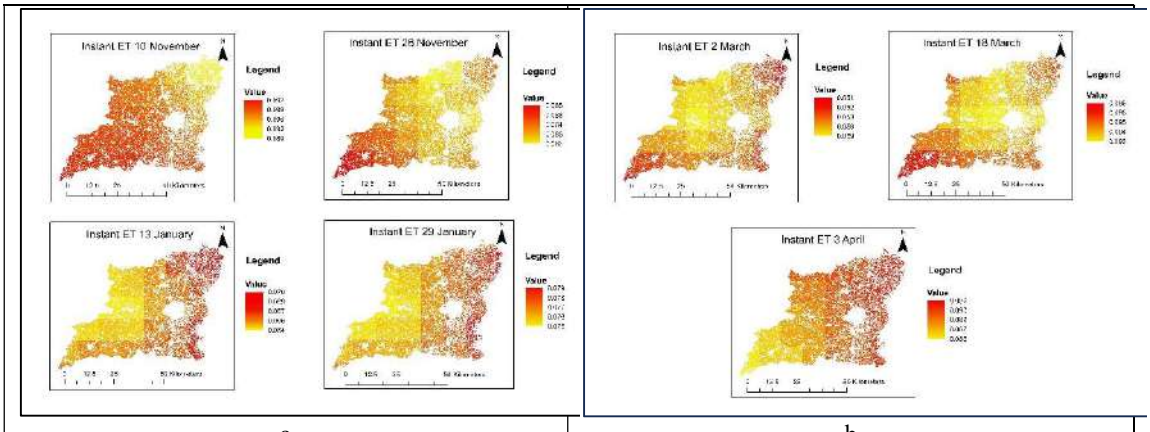

a b

Figure 4 Instantaneous ET from November to April

4.2. Estimation of Actual ET

The given maps in Figure 5 (a to g), show Actual Evapotranspiration (Evapotranspiration) for the Karnal district over various dates during the Rabi season. Every map displays Evapotranspiration spatial variability (in mm/day or mm),

International Journal of Information Technology & Computer Engineering
ISSN 2347–3657
Volume 14, Issue 1, 2026

demonstrating the dynamic water loss from crops and soil over time due to transpiration and evaporation.

The Figure 5a to d show early to mid-Rabi season maps from November 10 to January 29. On November 10, Evapotranspiration values ranged from 2.39 to 2.97 mm/day, which is relatively high and may be attributed to early crop irrigation or increased soil evaporation following sowing. By November 26, Evapotranspiration values decreased slightly to a range of 1.97–2.57 mm/day, likely reflecting the onset of crop establishment and reduced evaporation from exposed soil surfaces. Maps from January 13 and 29 (Figure 5c & 5d) show mid-season Evapotranspiration values between 1.59 and 2.50 mm/day, indicating moderate water use by the crop under cooler winter conditions. The Evapotranspiration for March 2, March 18, and April 3 is displayed in the Figure 5e to 5g. With Evapotranspiration values ranging from 0.59 to 0.80 on March 2, there is comparatively less water loss, which is indicative of cooler weather or early-to-mid crop stages. Evapotranspiration rises to 0.73–1.05 by March 18th, indicating an increase in water demand brought on by crop growth and warmer temperatures. Evapotranspiration peaks between 0.78 and 1.14 on April 3, indicating that crops nearing maturity use a lot of water due to increased transpiration and solar radiation.

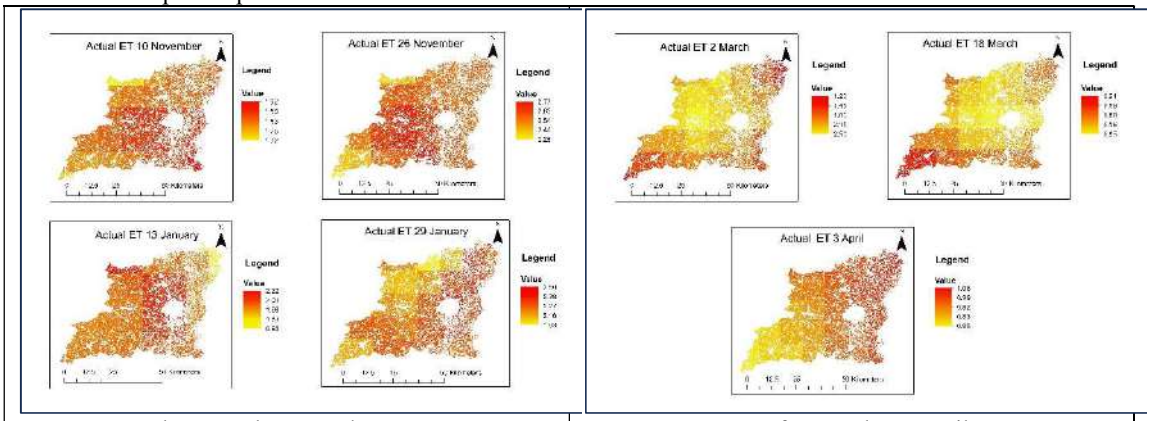

a & b November, c & d- January, e & f – March, g- April

Figure 5 Actual ET from November to April

4.3. Estimation of ET Based on Crop Coefficient Approach

The temporal variation of Actual Evapotranspiration (ETc) was analyzed to evaluate crop water requirements using the Crop Coefficient (Kc) approach of ET estimation. The Table 3 illustrates the crop evapotranspiration derived from pan evaporation data through crop coefficient approach spanning from November 2024 to April 2025. During March–April, evapotranspiration rises sharply due to increased temperature and wind acting on wheat field. The actual ET reduces as the wheat crop reaches maturity and senescence, lowering transpiration.

Table 4 Crop Evapotranspiration from Pan Evaporation Data

Date	Pan (mm)	Evaporation Pan Factor	Reference ET (mm)	Kc	Crop ET (mm)
10-Nov	2.4	0.75	1.8	0.7	1.26
26-Nov	1.3	0.75	1.05	1.15	1.12125
13-Jan	1.9	0.75	1.425	1.15	1.08
29-Jan	2.6	0.75	1.95	0.25	0.4875
2-Mar	1.9	0.75	1.425	0.25	0.35625
18-Mar	3.7	0.75	2.775	0.25	0.69375
3-Apr	5.2	0.75	3.9	0.25	0.975

4.4. Evaluation of METRIC Model

The observed Evapotranspiration obtained using the crop coefficient (Kc) approach and the METRIC-estimated actual Evapotranspiration as well as the statistical validation were shown in Table 4.

The validation results show average performance of the METRIC model with RMSE of 0.824 mm/day

International Journal of Information Technology & Computer Engineering
ISSN 2347–3657
Volume 14, Issue 1, 2026

and MAE of 0.609 mm/day. The model overestimated the ET values for 26 November and 13 January, which result the lower values of RMSE and MAE. The relatively low RMSE and MAE values further support the model's accuracy in estimating daily Evapotranspiration.

The coefficient of determination (R^2) between the observed and METRIC ET was displayed in Figure 6. The METRIC model has good agreement with the observed ET with an R^2 value of 0.68. This suggests a moderate to strong correlation, which means that the METRIC model outputs can account for roughly 68% of the variability in the observed Evapotranspiration.

This R2 value is regarded as acceptable in remote sensing-based Evapotranspiration estimation, especially in heterogeneous agricultural landscapes, even though it is not particularly high. This moderate performance can be attributed to a number of factors, including local microclimatic variations, atmospheric corrections, and sensor resolution.

Table 4 Statistical Validation of METRIC ET to the Observed ETc

Date	Observed ET (x)	METRIC ET (y)
10-Nov	1.26 ±0.35	1.96 ±0.85
26-Nov	1.12 ±0.35	2.77 ±0.85
13-Jan	1.08 ±0.35	2.23 ±0.85
29-Jan	2.24 ±0.35	2.92 ±0.85
02-Mar	1.63 ±0.35	2.93 ±0.85
18-Mar	0.69 ±0.35	0.91 ±0.85
03-Apr	0.97 ±0.35	1.05 ±0.85
SD	0.35	0.85
RMSE	**0.824**	
MAE	**0.609**	

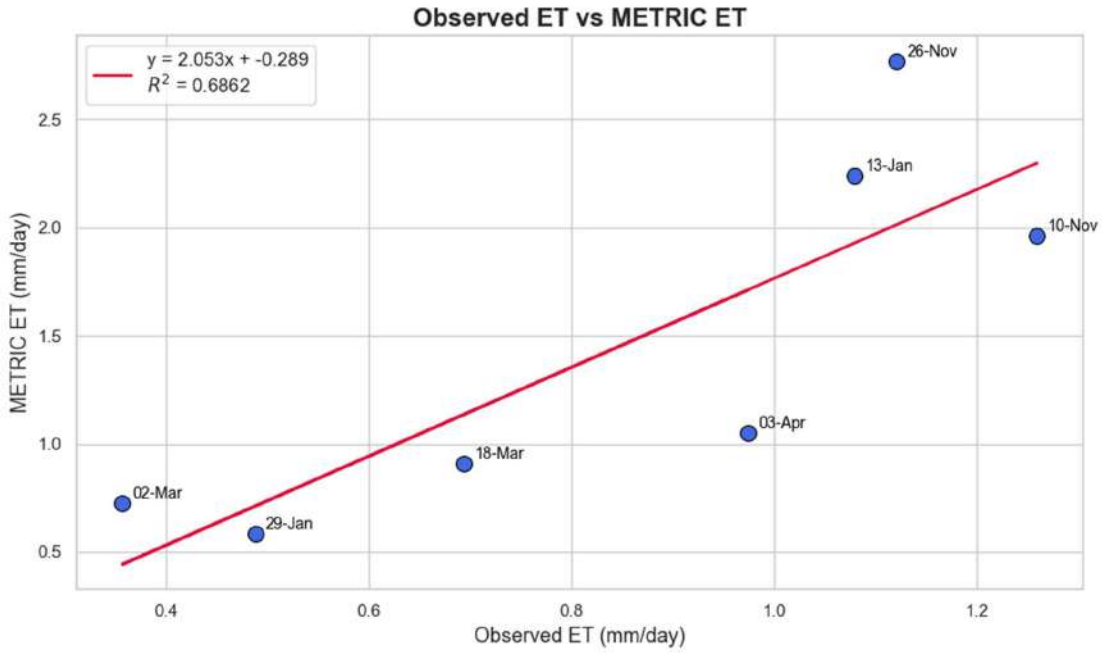

Figure 6 Coefficient of Determination Between METRIC ET and Observed ET

5. Discussion

METRIC demonstrated the model's ability to account for crop development stages and climatic influences by successfully capturing temporal and spatial variations in Evapotranspiration. For instance, peak evapotranspiration values coincided with the midseason growth stage, when water demand is at its highest. These trends are comparable to those noted by Gangwar et al. (2021), who used remote sensing to document seasonal evapotranspiration variability in wheat fields. ET generated by the METRIC model was similar to

those reported by Ch´avez et al. (2007), Santos et al. (2008), Folhes et al. (2009), Droogers et al. (2010), Healey et al. (2011), and Zhang et al. (2018), where they reported the spatial and temporal distribution of daily Eta for different crops.

A solid standard for validation was offered by the comparison with the Kc approach, which was based on the FAO Penman-Monteith method. The fact that ETc and METRIC-derived evapotranspiration agree suggests that METRIC can be a useful substitute for traditional techniques that rely heavily on meteorological inputs. According to Asadi et al. (2022), METRIC model performed well compared to SEBAL and ALARM with low RMSE values (0.761mm/day). Kapoor et al. (2022) conducted a comparative study of the METRIC and SEBAL (Surface Energy Balance Algorithm for Land) models, assessing their applicability in Indian agricultural contexts. Their research found that METRIC provided more accurate ET estimates due to its internal calibration mechanism, which minimizes errors from input data variability. Nain et al. (2023) conducted a detailed accuracy assessment of the METRIC model, validating its estimates of actual ET against ground-based measurements in wheat fields. The study confirmed the reliability and precision of the METRIC model, underscoring its applicability in agricultural water management. Comparison of ETa from the METRIC model with in situ atmometer readings in South Dakota by Reyes-González et al., (2017) showed strong agreement (r^2 = 0.87, d = 0.84, RMSE = 0.65 mm day^{-1}). In the western Urmia Lake Basin (2014–2016), METRIC-estimated ET showed reasonable accuracy with MAE of 0.57–0.72 mm d^{-1} and RMSE of 0.68–0.84 mm d^{-1} (Tasumi et al., 2019). These findings highlight the reliability of METRIC for local irrigation water management.

6. Conclusion

The study demonstrated the efficacy of the METRIC (Mapping evapotranspiration at high resolution with internalized calibration) Model in estimating actual evapotranspiration of crops in Karnal district of Haryana. The METRIC model applied in this study estimated actual evapotranspiration (ETa) for wheat crop across different growth stages in Karnal district. ETa values ranged between approximately 0.2 mm/day during initial stages and up to 5.2 mm/day during peak growth periods (mid-season stage), with spatial variability across the district. The METRIC-derived ETa maps effectively captured temporal dynamics corresponding to wheat phenology, confirming the model's suitability for local agro-climatic conditions.

Through the combination of ground-based meteorological inputs and satellite-derived biophysical parameters, METRIC produced spatially distributed Evapotranspiration estimates that exhibited with crop coefficient (Kc) calculations conducted in the field. The Model Validation yielded on R2 of 0.686, a RMSE of 0.824 mm/day and a mean absolute error (MAE) of 0.609 mm/day, indicating a satisfactory level of accuracy in capturing Evapotranspiration dynamics. This study demonstrates the utility of the METRIC model in accurately estimating actual evapotranspiration (ETa) for wheat crops; however, future research can expand its application to other major crops across different agro-climatic zones. Integration with high-temporal-resolution satellite data (e.g., Sentinel-2, MODIS) and real-time weather sensors will enhance temporal monitoring. The methodology can support regional-scale irrigation planning and water budgeting under climate change scenarios.

Reference:

1. Ahlawat, I. A., Sheoran, H. S., & Sihag, P. (2020). Analysis of Sentinel-1 data for regional crop classification: A multi-data approach for Rabi crops of district Hisar (Haryana). Journal of Applied and Natural Science, 12(2), 165–170. https://doi.org/10.31018/JANS.V12i2.2263
2. Allen, R. G., Bastiaanssen, W. G. M., Tasumi, M., Trezza, R., & Waters Consulting. (2002, August). Surface Energy Balance Algorithm for Land (SEBAL): Idaho implementation. Advanced training and user manual (Version 1.0) [Technical manual]. University of Idaho WaterWatch; Waters Consulting. https://posmet.ufv.br/wp-content/uploads/2017/04/MET-479-Waters-et-al-SEBAL.pdf
3. Asadi, M., & Kamran, K. V. (2022). Comparison of SEBAL, METRIC, and ALARM algorithms for estimating actual evapotranspiration of wheat crop. Theoretical and Applied Climatology, 149(1-2), 327-337.
4. Chauhan, K. K., & Lunagaria, M. M. (2024). Validation of biophysical parameters of wheat retrieved from Sentinel-2 data using in-situ measurements at Anand region of India. International Journal of Environment and Climate Change, 14(1), 626–638. https://doi.org/10.9734/IJECC/2024/v14i13878
5. Chavez, J. L., Gowda, P. H., Evett, S. R., Colaizzi, P. D., Howell, T. A., & Marek, T. (2007). An application of METRIC for ET mapping in the Texas high plains. Trans ASABE (submitted).
6. Droogers, P., Immerzeel, W. W., & Lorite, I. J. (2010). Estimating actual irrigation application by remotely sensed evapotranspiration observations. Agricultural Water Management, 97(9), 1351-1359.
7. Elhag, M., Psilovikos, A., Manakos, I., & Perakis, K. (2011). Application of the SEBS water balance model in estimating daily evapotranspiration and evaporative fraction

from remote sensing data over the Nile Delta. Water Resources Management, 25, 2731–2742. https://doi.org/10.1007/s11269-011-9824-1

8. Folhes, M. T., Rennó, C. D., & Soares, J. V. (2009). Remote sensing for irrigation water management in the semi-arid Northeast of Brazil. Agricultural Water Management, 96(10), 1398-1408.
9. Healey, N. C., Irmak, A., Arkebauer, T. J., Billesbach, D. P., Lenters, J. D., Hubbard, K. G., ... & Kjaersgaard, J. (2011). Remote sensing and in situ-based estimates of evapotranspiration for subirrigated meadow, dry valley, and upland dune ecosystems in the semi-arid sand hills of Nebraska, USA. Irrigation and drainage systems, 25(3), 151-178.
10. Hussain, S., Elfeki, A. M., Chaabani, A., Yibrie, E. A., & Elhag, M. (2022). Spatio-temporal evaluation of remote sensing rainfall data of TRMM satellite over the Kingdom of Saudi Arabia. Theoretical and Applied Climatology, 150(1), 363–377. https://doi.org/10.1007/s00704-022-03938-9
11. Pereira, L. S., Perrier, A., Allen, R. G., & Alves, I. (1999). Evapotranspiration: Concepts and future trends. Journal of Irrigation and Drainage Engineering, 125(2), 45–51. https://doi.org/10.1061/(ASCE)0733-9437(1999)125:2(45)
12. Prakash, R., Kumar, V., & Singh, A. (2021). Mapping evapotranspiration to evaluate irrigation efficiency in Indian wheat systems.
13. Qiu, R., Li, L., Liu, C., Wang, Z., Zhang, B., & Liu, Z. (2022). Evapotranspiration estimation using a modified crop coefficient model in a rotated rice–winter wheat system. Agricultural Water Management, 264, 107501. https://doi.org/10.1016/j.agwat.2022.107501
14. Reyes-González, A., Kjaersgaard, J., Trooien, T., Hay, C., & Ahiablame, L. (2017). Comparative analysis of METRIC model and atmometer methods for estimating actual evapotranspiration. International Journal of Agronomy, 2017(1), 3632501.
15. Roy, D. P., Wulder, M. A., Loveland, T. R., et al. (2014). Landsat-8: Science and product vision for terrestrial global change research. Remote Sensing of Environment, 145, 154–172. https://doi.org/10.1016/j.rse.2014.02.001
16. Santos, C., Lorite, I. J., Tasumi, M., Allen, R. G., & Fereres, E. (2008). Integrating satellite-based evapotranspiration with simulation models for irrigation management at the scheme level. Irrigation Science, 26(3), 277-288.
17. Senkondo, W., Munishi, S. E., Tumbo, M., Nobert, J., & Lyon, S. W. (2019). Comparing remotely-sensed surface energy balance evapotranspiration estimates in heterogeneous and data-limited regions: A case study of Tanzania's Kilombero Valley. Remote Sensing, 11(11), 1289. https://doi.org/10.3390/rs11111289
18. Singh, R. P., Paramanik, S., Bhattacharya, B. K., & Behera, M. D. (2020). Modelling of evapotranspiration using land surface energy balance and thermal infrared remote sensing. Tropical Ecology, 61, 282–295. https://doi.org/10.1007/s42965-020-00076-8
19. Steiner, J. L., Howell, T. A., & Schneider, A. D. (1991). LysiMETRIC evaluation of daily potential evapotranspiration models for grain sorghum. Agronomy Journal, 83(1), 240–247. https://doi.org/10.2134/agronj1991.00021962008300020026x
20. Tasumi, M. (2019). Estimating evapotranspiration using METRIC model and Landsat data for better understandings of regional hydrology in the western Urmia Lake Basin. Agricultural Water Management, 226, 105805.
21. Zhan, C., & Liang, S. (2021). Improved estimation of the global top-of-atmosphere albedo from AVHRR data. Remote Sensing of Environment, 262, 112514. https://doi.org/10.1016/j.rse.2021.112514
22. Zhang, H., Anderson, R. G., & Wang, D. (2015). Satellite-based crop coefficient and regional water use estimates for Hawaiian sugarcane. Field Crops Research, 180, 143-154.